Effect of Pore-Distributed Coke on Catalyst Regeneration Kinetics

Prior experimental study by Haldeman and Botty has demonstrated that catalyst regeneration rates vary with conversion, showing a nearly constant rate of reaction in the early stages of regeneration and falling off rapidly at higher conversion levels. This peculiar reaction behavior calls for explanation in terms of pore structural changes. In this work a mathematical model is developed based on the interaction between catalyst pore structure and coke distribution in the pores. The model is able to associate overall regeneration kinetics with alternative pore-distributed coke deposition patterns. Results exhibit a slight shallow rate maximum at an intermediate conversion level, in agreement with the prior experimental report. The model makes coke distribution in the pores accessible to experimental determination. The numerical results indicate that among pore structures with the same mean and overall pore volume, a larger variance offers a higher threshold for coke loading; for a given degree of dispersion, a smaller mean allows a higher coke loading.

Yuli Chang, D. D. Perlmutter
Department of Chemical Engineering
University of Pennsylvania
Philadelphia, PA 19104

Introduction

The high molecular weight condensed carbonaceous deposit that forms on the surface of cracking catalyst is commonly referred to as (catalytic) coke. Whether because of poisoning of the catalyst active sites or the changes in catalyst pore structure, coke deposition substantially reduces the effective catalyst activity. Mathematical modeling of the coking process can quantify the impact of coke deposition on catalyst activity.

One approach has expressed the loss of catalyst activity empirically in terms of a deactivation of catalytic sites (Voorhies, 1945; Froment and Bischoff, 1961, 1962; Weekman, 1969; Weekman and Nace, 1970; Sandana and Doraiswamy, 1971; Levenspiel, 1972; John et al., 1974; Wojciechowski, 1974). While this approach has given important insights into the kinetics of the process, it does not call for understanding of the nature of coke deposition. Another approach, more fundamental and systematic, expresses the loss of catalyst activity in terms of the catalyst pore structure and the coke deposit structure (Newson, 1975; Androutsopoulos and Mann, 1978; Hughes and Mann, 1978; Beeckman and Froment, 1979, 1980; El-Kady and Mann, 1981; Mann et al., 1984, 1985). It is then possible to consider a deactivation mechanism dominated by the changes in catalyst pore structure.

One shortcoming of the latter approach is that the geometry of the coke deposit structure must be assumed, since there is very little information available on the actual deposit structure in pores. In the analyses of Mann and his coworkers for instance, a wedge-layering model was adopted to describe the coke deposit structure in a cylindrical pore. It was the intention of this work to make the coke deposit structure accessible to experimental determination. For this purpose, a modeling approach was undertaken to use experimental pore structure data to characterize the pattern of coke deposition in pores and to relate this pore-distributed coke profile to the overall regeneration kinetics.

In the following a nonintersecting pores model is used. This is a common, mathematically convenient simplification for catalyst pore structure that has been widely adopted in characterizing porous material by interpreting data from pore structure measurement techniques such as vapor sorption and mercury porosimetry. The model results are not affected by the pore structure model assumed, so long as all the coke is accessible to the reactant fluid in the absence of occlusion of pore space by coke deposition. Only with coke loading in excess of that under consideration here would one expect occlusion of pore space by coke deposition to occur. Then results could indeed be affected by the pore structure assumed.

Background

Haldeman and Botty (1959) published observations for overall coke burning kinetics using particles of coked silica-alumina cracking catalyst. They worked with thoroughly aged coked catalyst samples, those that had been purged with an inert gas at regeneration temperature until a steady catalyst weight had been reached in order to remove the volatile hydrogen-rich material from the coke deposit. This so-called fast coke (Prater et al., 1983) can cause a rapid temperature rise in the beginning of regeneration, leading to an uncontrollable high initial reaction rate.

Under conditions of negligible mass transport resistance, Haldeman and Botty found that coke burning rates for those thoroughly aged coked catalyst particles varied with conversion, showing a nearly constant burning rate in the initial stages of regeneration, as presented in Figure 1. The coke burning rate function shown in Figure 1 was defined by the rate equation

$$-\frac{d}{dt}\,(C/C_0) = F(C/C_0)\,P_{ox}^{0.75} \exp\,[(-34{,}500)/RT] \quad (1)$$

Haldeman and Botty further found $F(C/C_0)$ to be independent of the initial level of coke loading between 0.5 and 6 wt. %, implying that the carbonaceous phase in the catalyst exists in approximately the same state of aggregation regardless of initial coke content. However, this observation is inconsistent with the fact that coke burning rates exhibit a nearly constant rate of reaction in the early stages of regeneration. Had indeed the coke burning rate function $F(C/C_0)$ been independent of the initial coke level, the reaction rate would be linear in the amount of coke deposited on the catalyst, and coke burning rates would decrease monotonically with conversion. Haldeman and Botty attributed the nearly constant rate of reaction between coke conversions of 0.1 and 0.5 to the development of inner surface as coke is consumed during oxidation.

Pore volume distributions for the coked and uncoked catalysts were also given in the same work. These pore volume distributions, shown in Figure 2, were computed from the desorption branch of the nitrogen sorption isotherms according to the method of Barrett et al. (1951), based on a nonintersecting cap-

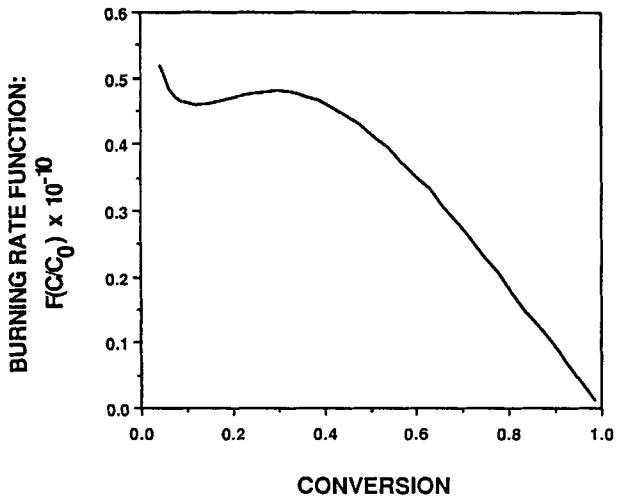

Figure 1. Regeneration data (Haldeman and Botty, 1959).

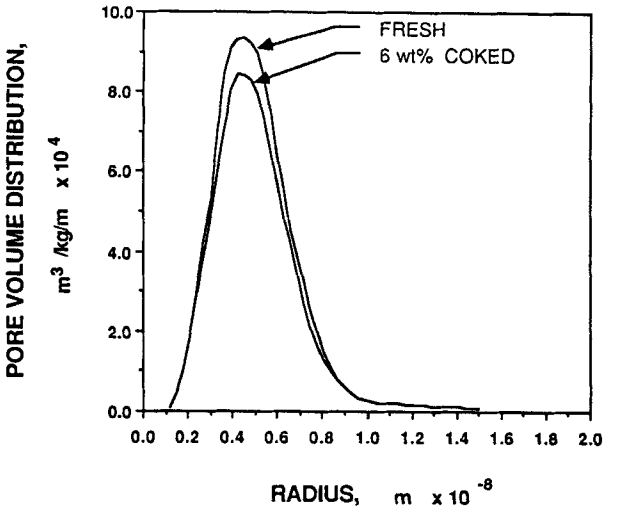

Figure 2. Pore structure data (Haldeman and Botty, 1959).

illaries model of catalyst pore structure in which the capillaries, although not necessarily cylinders, have circular cross sections. The similarity in the shape and magnitude of these pore volume distributions indicates that there is negligible occlusion of catalyst pore space by coke deposition. Haldeman and Botty attempted to obtain the distribution of coke in the pores by taking the difference between the two pore volume distributions in Figure 2; however, this is only a rough estimate because the pores that have the same radial pore size in the coked and uncoked catalyst are not strictly the same pores.

That kinetics can vary with conversion in accordance with the development of new inner reactive surface has been observed for other heterogeneous gas-solid reactions such as char gasification and carbon activation. Like catalyst regeneration, these reactions also involve partial oxidation of a carbonaceous surface. A variety of studies (Jenkins et al., 1973; Hippo and Walker, 1975; Tomita et al., 1977; Dutta et al., 1977; Dutta and Wen, 1977; Hashimoto et al., 1979; Chin et al., 1983; Su and Perlmutter, 1985) have demonstrated that measured reaction rates change with conversion, showing a maximum rate at an intermediate conversion level. The physical structure of the solid reactant also changes continuously as reaction proceeds, and this evolution of pore structure affects the reaction kinetics by altering the available reaction surface area.

To account for this effect of the structural changes, a random pore model was proposed by Bhatia and Perlmutter (1980), and independently by Gavalas (1980), that interprets conversion data and the changes of reaction surface area in terms of a combination of chemical and pore size effects. This random pore model expresses reaction rate as

$$-\frac{dX}{d\tau} = \frac{S}{S_0} = (1 - X)\,\sqrt{1 - \Psi \ln (1 - X)} \quad (2)$$

where τ is a kinetic time parameter and Ψ is a structure parameter dependent on initial surface, porosity, and pore length.

Successful application of the random pore model has been demonstrated for char gasification (Bhatia and Perlmutter, 1980; Su and Perlmutter, 1985); however, interpretation of catalyst regeneration kinetics via this model is complicated by the

solid phase involved in the catalyst regeneration reaction system. The major difference between reactions such as char gasification or carbon activation on the one hand, and regeneration of coked catalyst on the other, is that the solid phase on which the former two reactions occur is relatively homogeneous, whereas that for the latter is not.

Since the coked catalyst contains both reactive coke deposit (reacting material) and a nonreactive catalyst matrix (inert substance), a model is needed that accounts for the interaction between the catalyst pore space and the space occupied by the coke deposit. In the development that follows no specification is needed as to the coke deposit geometry in the pores.

Model Development

Consider the solid phase participating in a fluid-solid reaction to be a composite solid consisting of a major portion of inert substance (catalyst) and a small portion of reacting material (coke). The inert substance functions as a support on which the reacting material is deposited. The isothermal chemical reaction takes place between A, the solid reacting material (coke) deposited on the walls of pores in the inert support, and a fluid B, according to the stoichiometry of the equation

$$a\,A_{(s)} + b\,B_{(g)} \rightarrow p\,P_{(g)} + q\,Q_{(g)} + \cdots \qquad (3)$$

If all the internal surface of the inert support were covered by the reacting material, the composite solid would behave as if it were composed only of the reacting material, since the reactant fluid would not be able to contact the inert support underneath the layer of the reacting material. The reaction is initiated on the inner surfaces of the pores in the composite solid. As reaction progresses, each pore of the particle has associated with it a growing reaction surface, which initially corresponds to the inner surface of the pore. As the pores enlarge and the various reaction surfaces in the particle grow, islands of nonreacting surface of the inert support will emerge as the reacting material covering them is consumed. After the emergence of the inert surface, the pores stop enlarging and development of the overall surface area of the particle will slow down. This pore development process is illustrated in Figure 3. It is assumed that the pore space of the composite solid is not blocked by the reacting material.

Consider the pores in the inert support to be a bundle of nonintersecting pores, each with a circular cross section but not necessarily a cylinder, and consider the radial pore sizes to be described by a measurable pore volume distribution function $f(r)$, where $f(r)dr$ is the contribution to the overall pore volume in the inert support arising from portions of pores that have radii between r and $r + dr$. The cumulative pore volume, pore surface area, and pore length are determined via the pore volume distribution function by

$$V = \int_{r_N}^{r_W} f(r)\,dr \qquad (4)$$

$$S = 2\int_{r_N}^{r_W} \frac{f(r)}{r}\,dr \qquad (5)$$

and

$$L = \frac{1}{\pi}\int_{r_N}^{r_W} \frac{f(r)}{r^2}\,dr \qquad (6)$$

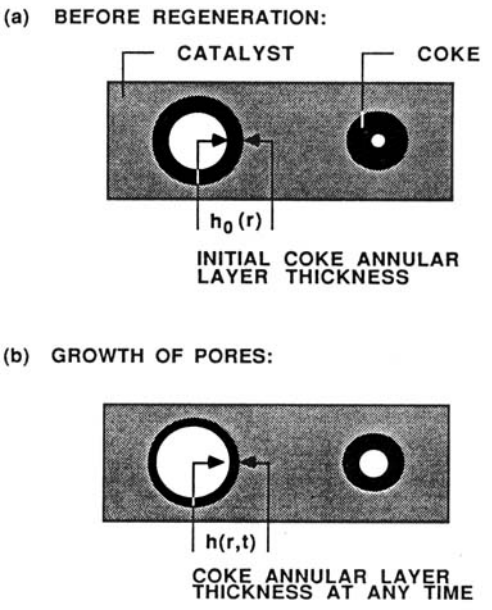

Figure 3. Pore structure development within a solid phase containing a major portion of inert substance.

respectively, where the range of radial pore size only exists between a smallest radius r_N and a largest radius r_W. It should be noted that the integrands $f(r)/r$ and $f(r)/r^2$ in Eqs. 5 and 6 are called, respectively, the pore surface area distribution function and the pore length distribution function of the pores in the inert support.

Consider the volumes of reacting material deposited on the inner surfaces of pores in the inert support to be described by a volume distribution function $g(r)$, for which $g(r)dr$ is the contribution arising from the coke deposited on the inner surfaces of pores that have radii between r and $r + dr$. Thus, the overall volume of reacting material is determined from the volume distribution function by the integral

$$V_R = \int_{r_N}^{r_W} g(r)\,dr \qquad (7)$$

Using the expression for the volume of an annulus

$$g(r)dr = \pi\{r^2 - [r - h_0(r)]^2\}\,dL \qquad (8)$$

where dL is the differential pore length

$$dL = \frac{f(r)}{\pi r^2}\,dr \qquad (9)$$

and $h_0(r)$ is the initial annular layer thickness of reacting material, i.e., the pore-distributed profile of the reacting material. Combining Eqs. 8 and 9 and rearranging gives

$$h_0(r) = \left[1 - \sqrt{1 - \frac{g(r)}{f(r)}}\right] r \tag{10}$$

It must be emphasized that neither $g(r)$ nor $h_0(r)$ is directly measurable, and another approach is needed to make $g(r)$ or $h_0(r)$ accessible to experimental determination.

The growth of the total reaction surface in the composite may be followed in terms of the radial growth of a given set of nonintersecting pores, as shown in Figure 3b. If the rate of reaction on the actual surface is proportional to the total surface area:

$$\frac{d}{dt}[h(r, t)] = -R_s \tag{11}$$

Integrating Eq. 11, one obtains

$$h(r, t) = \begin{cases} h_0(r) - R_s t, & t \le t^*(r) \\ 0, & t > t^*(r) \end{cases} \tag{12}$$

where $t^*(r)$ denotes the time period required for the coke to be consumed from the inner surfaces of pores that have radii between r and $r + dr$, i.e.,

$$t^*(r) = \frac{h_0(r)}{R_s} \tag{13}$$

Figure 3c shows schematically the emergence during reaction of the surface of the inert support.

The differential reacting material volume at any time in the portions of pores that have radii between r and $r + dr$ is:

$$dv = \{r^2 - [r - h(r, t)]^2\} \frac{f(r)}{r^2}\, dr \tag{14}$$

Integrating with respect to r gives the overall volume of coke in the composite at any time as:

$$V_R^*(t) = \int_{r_N}^{r_W} \{r^2 - [r - h(r, t)]^2\} \frac{f(r)}{r^2}\, dr \tag{15}$$

From the definition of conversion:

$$1 - X = \frac{V_R^*(t)}{V_R} \tag{16}$$

Thus the conversion-time relationship of the fluid-solid reaction is:

$$X = 1 - \frac{1}{V_R} \int_{r_N}^{r_W} \{r^2 - [r - h(r, t)]^2\} \frac{f(r)}{r^2}\, dr \tag{17}$$

Upon combination with Eqs. 10, 12, and 13, Eq. 17 becomes

$$X = 1 - \frac{1}{V_R} \int_{r_N}^{r_W} P(r, t) \frac{f(r)}{r^2}\, dr \tag{18}$$

where

$$P(r, t) = \begin{cases} r^2 - \left[r\sqrt{1 - \dfrac{g(r)}{f(r)}} + R_s t\right]^2, & t \le \dfrac{r\left[1 - \sqrt{1 - \dfrac{g(r)}{f(r)}}\right]}{R_s} \\ 0, & t > \dfrac{r\left[1 - \sqrt{1 - \dfrac{g(r)}{f(r)}}\right]}{R_s} \end{cases} \tag{19}$$

Differentiating Eq. 18 with respect to time gives

$$\frac{dX}{dt} = \frac{2 R_s}{V_R} \int_{r_N}^{r_W} Q(r, t) \frac{f(r)}{r^2}\, dr \tag{20}$$

where

$$Q(r, t) = \begin{cases} r\sqrt{1 - \dfrac{g(r)}{f(r)}} + R_s t, & t \le \dfrac{r\left[1 - \sqrt{1 - \dfrac{g(r)}{f(r)}}\right]}{R_s} \\ 0, & t > \dfrac{r\left[1 - \sqrt{1 - \dfrac{g(r)}{f(r)}}\right]}{R_s} \end{cases} \tag{21}$$

In dimensionless form

$$X = 1 - \frac{1}{\bar{V}} \int_1^{\bar{r}_W} \bar{P}(\bar{r}, \tau) \frac{\bar{f}(\bar{r})}{\bar{r}^2}\, d\bar{r} \tag{22}$$

where

$$\bar{P}(\bar{r}, \tau) = \begin{cases} \bar{r}^2 - \left[\bar{r}\sqrt{1 - \dfrac{\bar{V}\bar{g}(\bar{r})}{\bar{f}(\bar{r})}} + \tau\right]^2, & \tau \le \bar{r}\left[1 - \sqrt{1 - \dfrac{\bar{V}\bar{g}(\bar{r})}{\bar{f}(\bar{r})}}\right] \\ 0, & \tau > \bar{r}\left[1 - \sqrt{1 - \dfrac{\bar{V}\bar{g}(\bar{r})}{\bar{f}(\bar{r})}}\right] \end{cases} \tag{23}$$

$$\frac{dX}{d\tau} = \frac{2}{\bar{V}} \int_1^{\bar{r}_w} \bar{Q}(\bar{r}, \tau) \frac{\bar{f}(\bar{r})}{\bar{r}^2} d\bar{r} \tag{24}$$

where

$$\bar{Q}(\bar{r}, \tau) = \begin{cases} \bar{r}\sqrt{1 - \frac{\bar{V}\bar{g}(\bar{r})}{\bar{f}(\bar{r})}} + \tau, & \tau \le \bar{r}\left[1 - \sqrt{1 - \frac{\bar{V}\bar{g}(\bar{r})}{\bar{f}(\bar{r})}}\right] \\ 0, & \tau > \bar{r}\left[1 - \sqrt{1 - \frac{\bar{V}\bar{g}(\bar{r})}{\bar{f}(\bar{r})}}\right] \end{cases} \tag{25}$$

The essential parameters of the proposed model are the overall volume of coke, V_R, and the functions $f(r)$ and $g(r)$, which are, respectively, the pore volume distribution of the inert porous media and the coke volume

The dimensionless variables in Eqs. 22 to 25 are defined as:

$$\bar{V} = \frac{V_R}{V} \tag{26}$$

$$\bar{r} = \frac{r}{r_N} \tag{27}$$

$$\tau = \frac{R_s t}{r_N} \tag{28}$$

$$\bar{f}(\bar{r}) = \frac{r_N}{V} f(r) \tag{29}$$

and

$$\bar{g}(\bar{r}) = \frac{r_N}{V_R} g(r) \tag{30}$$

Analysis

Coke volume distribution

To determine the pore-distributed profile of the reacting material $h_0(r)$, dictated by Eq. 10, one needs to relate $g(r)$ to the pore volume distribution of the inert support $f(r)$. Defining F_k by

$$F_k = \int_{r_N}^{r_w} \frac{f(r)}{r^k} dr \tag{31}$$

and multiplying by constant V_R/F_k on both sides gives:

$$V_R = \int_{r_N}^{r_w} \frac{V_R f(r)}{F_k r^k} dr \tag{32}$$

Comparison with Eq. 7 shows that one solution for $g(r)$ is

$$g(r) = V_R \frac{f(r)}{F_k r^k} \tag{33}$$

The index k involves specific assumptions on the manner of the deposition of reacting material in the pore space of the inert support, as will be discussed subsequently in the context of coke formation.

The coke-formation reactions involved in heterogeneous catalytic hydrocarbon cracking can vary considerably, and specific results depend on the species of hydrocarbon in the feed. Based on experimental evidence, Gates et al. (1979) have concluded that coke formation occurs as the product of a primary surface cracking reaction if the feed contains multiring aromatic hydrocarbons of high molecular weight. If on the other hand the feed contains no aromatic hydrocarbons, coke formation occurs as the product of a secondary reaction that involves the products formed from the primary cracking. With this in mind, deposition of coke in the pores could occur either by a heterogeneous cracking reaction or via a homogeneous vapor phase reaction.

If the deposition of coke occurs via the former mechanism, the amount of coke deposited in each size of pore would be proportional to its pore surface area, and therefore the coke volume distribution would be expected to be proportional to the pore surface area distribution of the uncoked catalyst. If instead the deposition of coke occurs via a homogeneous vapor phase reaction, and provided that counterdiffusion of the product of this reaction does not limit the overall rate, the amount of coke deposited in each size of pore would be proportional to its pore volume, and the resulting coke distribution would be proportional to the pore volume distribution of the catalyst. In the event, however, that counterdiffusion of one or more of the products of the homogeneous vapor phase reaction out of the pores is limiting, the amount of coke deposited in each size of pore would be dependent on the pore length. If the dependence is a linear relationship, the coke volume distribution would be proportional to the pore length distribution of the uncoked catalyst.

These considerations suggest three alternative models for the pore-distributed coke, each of which corresponds to one of the above-noted coking processes.

Case I. The coke volume distribution is proportional to the pore volume distribution of the catalyst, i.e., $k = 0$,

$$F_k = V \tag{34}$$

and

$$g(r) = \frac{V_R}{V} f(r) \tag{35}$$

Case II. The coke volume distribution is proportional to the pore surface area distribution of the catalyst, i.e., $k = 1$,

$$F_k = \frac{S}{2} \tag{36}$$

and

$$g(r) = \frac{2V_R}{S} \frac{f(r)}{r} \tag{37}$$

Case III. The coke volume distribution is proportional to the pore length distribution of the catalyst, i.e., $k = 2$,

$$F_k = \pi L \tag{38}$$

and

$$g(r) = \frac{V_R f(r)}{\pi L r^2} \tag{39}$$

The characteristics (the mean and variance) of these alternative coke volume distributions can be determined in terms of the catalyst pore structure. Define the mean (the centroid) and variance of the pore volume distribution of the catalyst as

$$\mu_f = \frac{\int_{r_N}^{r_W} rf(r)\,dr}{\int_{r_N}^{r_W} f(r)\,dr} \tag{40}$$

and

$$\sigma_f^2 = \frac{\int_{r_N}^{r_W} r^2 f(r)\,dr}{\int_{r_N}^{r_W} f(r)\,dr} - \mu_f^2 \tag{41}$$

respectively, and those of the coke volume distribution as

$$\mu_g = \frac{\int_{r_N}^{r_W} rg(r)\,dr}{\int_{r_N}^{r_W} g(r)\,dr} \tag{42}$$

and

$$\sigma_g^2 = \frac{\int_{r_N}^{r_W} r^2 g(r)\,dr}{\int_{r_N}^{r_W} g(r)\,dr} - \mu_g^2 \tag{43}$$

respectively. In addition, define

$$r_{E1} = \frac{2V}{S} \tag{44}$$

$$r_{E2} = \frac{S}{2\pi L} \tag{45}$$

where r_{E1} and r_{E2} denote the equivalent radii of cylinders that have the same V and S and the same S and L, respectively, as the pore structure of the catalyst. Multiplying by r^m on both sides of Eq. 33, where the index m is an integer, and integrating with respect to r gives:

$$\int_{r_N}^{r_W} r^m g(r)\,dr = \frac{V_R}{F_k}\int_{r_N}^{r_W} r^{m-k} f(r)\,dr \tag{46}$$

Combining with Eqs. 7 and 31 and rearranging gives

$$\frac{\int_{r_N}^{r_W} r^m g(r)\,dr}{\int_{r_N}^{r_W} g(r)\,dr} = \frac{\int_{r_N}^{r_W} r^{m-k} f(r)\,dr}{\int_{r_N}^{r_W} \frac{f(r)}{r^k}\,dr} \tag{47}$$

For case I ($k = 0$), $m = 1$ gives

$$\mu_g = \mu_f \tag{48}$$

and $m = 2$ gives

$$\sigma_g^2 + \mu_g^2 = \sigma_f^2 + \mu_f^2 \tag{49}$$

Combining with Eq. 48 gives

$$\sigma_g^2 = \sigma_f^2 \tag{50}$$

For case II ($k = 1$), $m = 1$ gives

$$\mu_g = \frac{\int_{r_N}^{r_W} f(r)\,dr}{\frac{S}{2}} = \frac{2V}{S} = r_{E1} \tag{51}$$

and $m = 2$ gives

$$\sigma_g^2 + \mu_g^2 = \frac{2\int_{r_N}^{r_W} rf(r)\,dr}{S} = \frac{2V}{S}\frac{\int_{r_N}^{r_W} rf(r)\,dr}{\int_{r_N}^{r_W} f(r)\,dr} = r_{E1}\mu_f \tag{52}$$

Combining with Eq. 51 and rearranging:

$$\sigma_g^2 = r_{E1}^2 \mu_f - r_{E1}^2 \tag{53}$$

For case III ($k = 2$), $m = 1$ gives

$$\mu_g = \frac{\int_{r_N}^{r_W} \frac{f(r)}{r}\,dr}{\int_{r_N}^{r_W} \frac{f(r)}{r^2}\,dr} = \frac{S}{2\pi L} = r_{E2} \tag{54}$$

and $m = 2$ gives

$$\sigma_g^2 + \mu_g^2 = \frac{\int_{r_N}^{r_W} f(r)\,dr}{\int_{r_N}^{r_W} \frac{f(r)}{r^2}\,dr} = \frac{V}{\pi L} = r_{E1} r_{E2} \tag{55}$$

Combining with Eq. 54 and rearranging:

$$\sigma_g^2 = r_{E1} r_{E2} - r_{E2}^2 \tag{56}$$

If the pore structure of the catalyst were indeed a single cylinder, the coke volume distribution and the pore volume distribution would be geometrically identical for all three cases.

Pore-distributed coke profile

On the basis of these alternative hypotheses, one can compute the dimensionless pore-distributed coke profile $\bar{h}_0(\bar{r})$ for each case of the distribution of reacting material from the equation

$$\bar{h}_0(\bar{r}) = \left[1 - \sqrt{1 - \frac{\bar{V}\bar{g}(\bar{r})}{\bar{f}(\bar{r})}}\right]\bar{r} \tag{57}$$

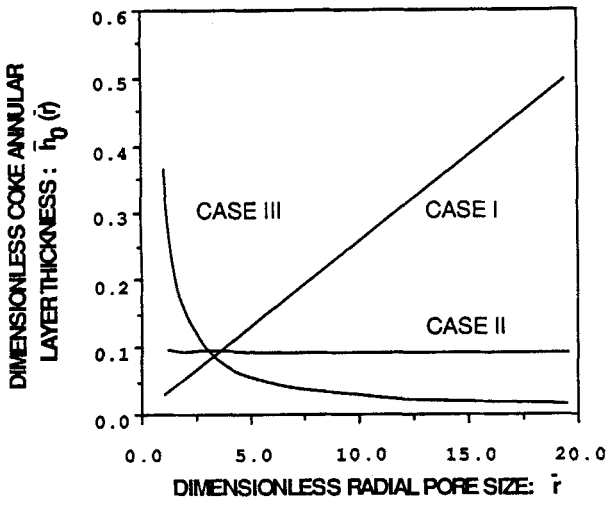

Figure 4. Effect of pore size on deposition of coke for various pore-distributed coke distributions.
Coke volume fraction $\bar{V} = 0.05$

The results are presented in Figure 4 in terms of the dimensionless radial pore size, for $\bar{V} = 0.05$.

The differences among the three cases that are shown in Figure 4 can have a significant impact on the way in which reaction rate changes with conversion. In case II, for example, the annular layer thickness of reacting material is about the same for all pore sizes. Consequently, the process of emergence of islands of nonreacting surface of the inert support is delayed until almost all the reacting material is consumed. As a result, the overall reaction surface associated with the pores increases until almost complete conversion. This is illustrated in Figure 5, in which the patterns of reaction behavior presented are computed results, determined by Eqs. 22 to 25, using the pore volume distribution of the uncoked catalyst of Haldeman and Botty (1959) and coke content = 3.36 wt. % (a convenient middle value over the range studied in the reference). Details of this calculation will be given later.

For cases I and III, the annular layer thickness of coke increases with larger and smaller pore sizes, respectively. Consequently, the process of emergence of islands of nonreacting surface of the inert support favors the small and the large pores for cases I and III, respectively. As a result, the overall reaction surface increases only to a certain conversion and from then on decreases. Thus, in Figure 5 slight shallow maxima in rate occur at an intermediate conversion level for cases I and III, arising from two opposing effects: the growth of reaction surfaces associated with the pores, and the loss of these surfaces associated with the depletion of the reacting material. These maxima in rate are not quite small numerically as compared with the experimental maximum. However, were the errors of the data of Haldeman and Botty within the limits of the usual experimental error, the maximum in rate observed would be much less pronounced.

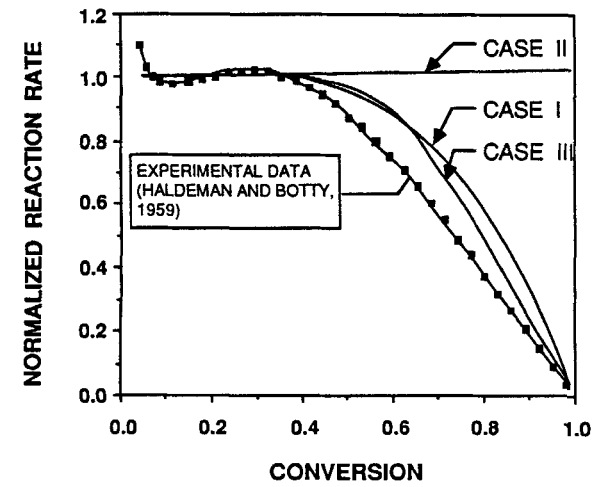

Figure 5. Development of reaction rate with conversion.
Data normalized with respect to rates at conversion = 0.075

Since for real solutions the discriminant in Eq. 35

$$D = 1 - \frac{\bar{V}\bar{g}(\bar{r})}{\bar{f}(\bar{r})} \tag{58}$$

must be greater than zero for all radial pore sizes,

$$\bar{V} < \frac{\bar{f}(\bar{r})}{\bar{g}(\bar{r})} \tag{59}$$

By substituting the defining normalizing Eqs. 29 and 30

$$\bar{V} < \frac{F_k r^k}{V} \tag{60}$$

Since the inequality of Eq. 60 must satisfy all radial pore sizes,

$$\bar{V} < \frac{F_k r_N^k}{V} \tag{61}$$

Combining with Eq. 31 and by substituting the defining Eqs. 27 and 29,

$$\bar{V} < \int_1^{\bar{r}_w} \frac{\bar{f}(\bar{r})}{\bar{r}^k}\, d\bar{r} \tag{62}$$

From the inequality of Eq. 62 one obtains the criterion for no blockage of pore space in the catalyst for cases I, II, and III. Below this critical value of $\bar{V}$ no occlusion of pore space in the catalyst will occur.

For case I, the critical value of $\bar{V}$ is always equal to unity independent of the pore volume distribution; that is, no blockage of pores in the catalyst can occur before all the pore space is filled.

Results and Discussion

The patterns of reaction behavior of this model, given by Eqs. 22 to 25, may be compared with the experimental observations of Haldeman and Botty, if the required model parameters are extracted from their report. The details of these computations are summarized in Table 1. The pore volume distribution for the uncoked catalyst, shown in Figure 2, was used to read point values for $f(r)$, which were then scaled and normalized according to Eq. 29 using the data of Table 1. Coke distributions of cases I, II, and III, dictated by Eqs. 35, 37, and 39, respectively, were used as inputs for $g(r)$, which were scaled and normalized according to Eq. 30.

Table 1. Required Model Parameters Extracted from Data of Haldeman and Botty (1959)

Values given by Haldeman and Botty
$r_N = 1.2 \times 10^{-9}$ m
$r_W = 1.5 \times 10^{-8}$ m
$V = 4.2 \times 10^{-4}$ m^3/kg
$\rho = 1.6 \times 10^3$ kg/m^3

Value assumed
$C_0 = 3.36$ wt. % = 0.0336 kg/kg

Values calculated
From Eq. 27:
$\bar{r}_N = 1.0$ and $\bar{r}_W = 12.5$
From the definition of density:
$V_R = 0.0336/(1.6 \times 10^3) = 2.1 \times 10^{-5}$ m^3/kg
From Eq. 26:
$\bar{V} = (2.1 \times 10^{-5})/(4.2 \times 10^{-4}) = 0.05$

For comparison, the regeneration data of Haldeman and Botty are superimposed on the computed reaction rates in Figure 5. Both the predictive rates and the experimental rates were normalized with respect to the rate values at conversion = 0.075. The computed rates for cases I and III follow the trend of the experimental rate development, but the case II results differ sharply.

In order to discriminate between cases I and III for the distribution of coke, the criteria for no blockage of pore space computed for cases I and III may be compared with that derived from the experiments. Haldeman and Botty reported that there is no significant occlusion of catalyst pore space by coke deposition up to 6 wt. % (0.06 kg/kg). Weisz and Goodwin (1966) had already reported that coke was inaccessible to oxygen above 6 wt. % of coke loading. Using this transition value (6 wt. %) of coke loading together with the solid coke density $\rho = 1.6 \times 10^3$ kg/m^3 and the total pore volume $V = 4.2 \times 10^{-4}$ m^3/kg, one can estimate the critical value of $\bar{V}$ from Eq. 26: $\bar{V}_c = 0.06/(1.6 \times 10^3)/(4.2 \times 10^{-4}) = 0.0893$. For comparison, the critical $\bar{V}$ for cases I, II, and III are 1.0, 0.271, and 0.0836, respectively. The case III result is closest to the experimental estimation.

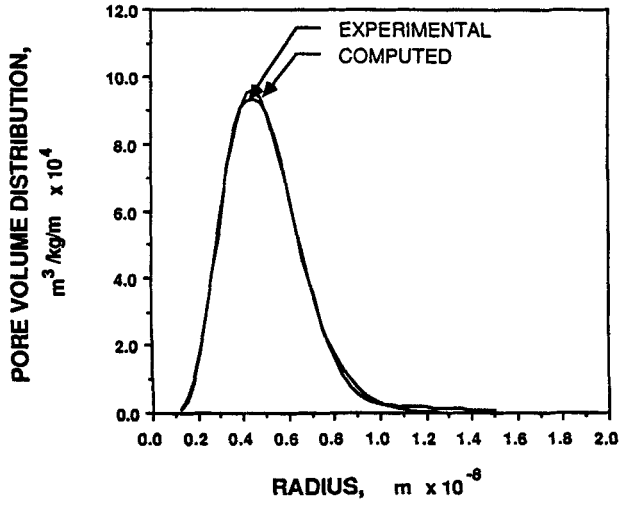

Figure 6. Computed pore volume distribution compared with experimental data of Haldeman and Botty (1959).

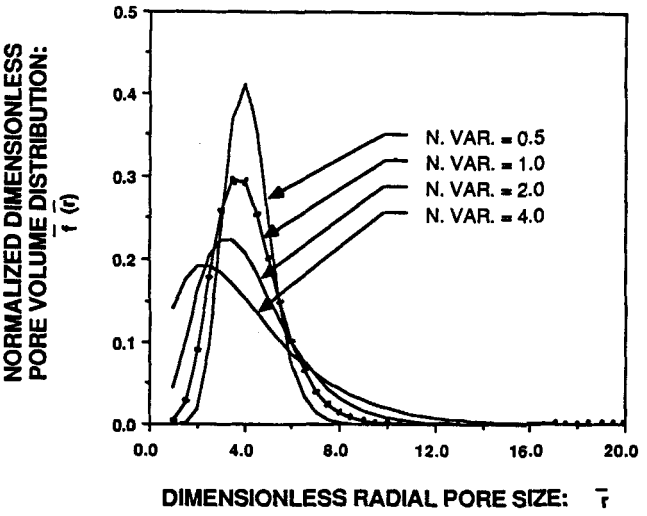

Figure 7. Gamma distributions with various variances.
N. Var., normalized mean

Combining the comparisons in the patterns of reaction behavior and the criterion for no blockage of pore space, one may conclude that case III best describes the coke distribution in the pores of the catalyst used in the experiments of Haldeman and Botty.

Pore structure effect

Accepting as most likely the coke distribution of case III, one can computationally study the effects of the pore volume distribution on coke loading as well as on catalyst regeneration kinetics. For this purpose it is convenient to fit the pore volume distribution of Haldeman and Botty with a two-parameter gamma distribution function given by

$$G(r) = \frac{\lambda^\rho r^{\rho-1} e^{-\lambda r}}{\Gamma(\rho)}, \quad r > 0 \tag{63}$$

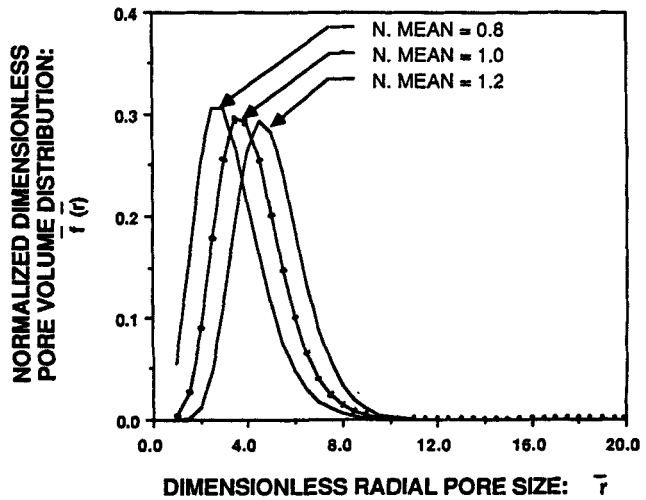

Figure 8. Gamma distributions with various means.
N. Mean, normalized mean

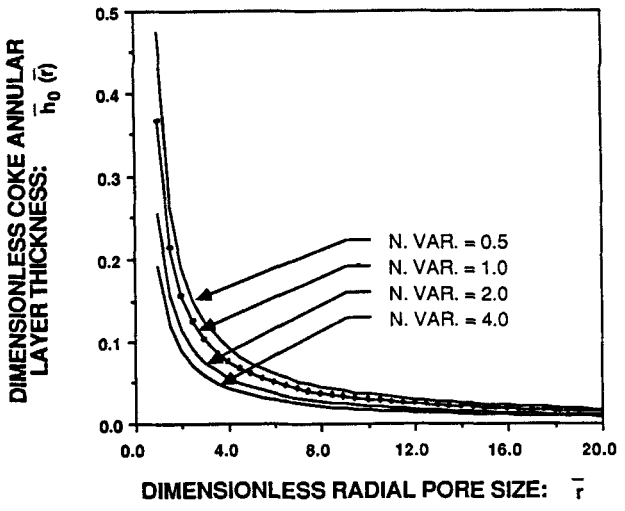

Figure 9. Coke profiles for various pore volume distributions.
Case III, coke volume fraction $\bar{V} = 0.05$.
N. Var., normalized variance

where the parameters ρ and λ are taken to be positive, and $\Gamma(\rho)$ denotes the Euler gamma function defined by

$$\Gamma(\rho) = \int_0^\infty t^{\rho-1} e^{-t}\, dt \tag{64}$$

The gamma distribution computed for the experimental curve via a nonlinear least-squares regression analysis (IMSL routine ZXSSQ) gave $\rho = 8.81$ and $\lambda = 2.12$. The result is presented in Figure 6, showing that the computed distribution agrees with the measured distribution within the limits of the usual experimental error.

Since the mean and the variance for the gamma distribution function are

$$\mu = \frac{\rho}{\lambda} \tag{65}$$

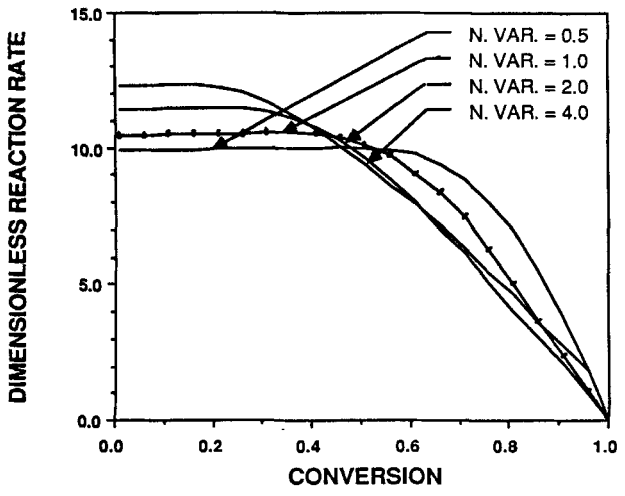

Figure 10. Effect of overall conversion on reaction rates for various pore volume distributions.
Case III, coke volume fraction $\bar{V} = 0.05$
N. Var., normalized variance

Table 2. Effect of Pore Structure on Criterion for No Blockage of Pore Space

Normalized Variance	Critical $\bar{V}$
0.5	0.0691
1.0	0.0836
2.0	0.1127
4.0	0.1442

and

$$\sigma^2 = \frac{\rho}{\lambda^2} \tag{66}$$

respectively, the mean and the variance for the distribution function can be changed independently. The results of such variations are shown in Figures 7 and 8, for which all the distribution functions have been normalized with respect to their areas over the same finite range of radial pore size. The dotted curve represents the gamma distribution computed for the normalized experimental data of Haldeman and Botty. Using these sets of pore volume distributions, one can place the experiments within the context of the model predictions.

The pore-distributed coke profiles computed for pore volume distributions with different variances are shown in Figure 9, based on the distributions shown in Figure 7 and for the coke volume fraction $\bar{V} = 0.05$. Since the overall pore length increases with the degree of dispersion in pore structure, and since case III distributes reacting material according to the overall pore length, the amount of coke per unit pore length should be smaller in a coked catalyst with a more dispersed pore structure. As a result, the coke layer is expected to be thinner in a more dispersed pore structure, as presented in Figure 9. This gives a larger reaction surface area in a coked catalyst with a more dispersed pore structure. This is illustrated in Figure 10, which shows that reaction rates increase with the variance in the pore

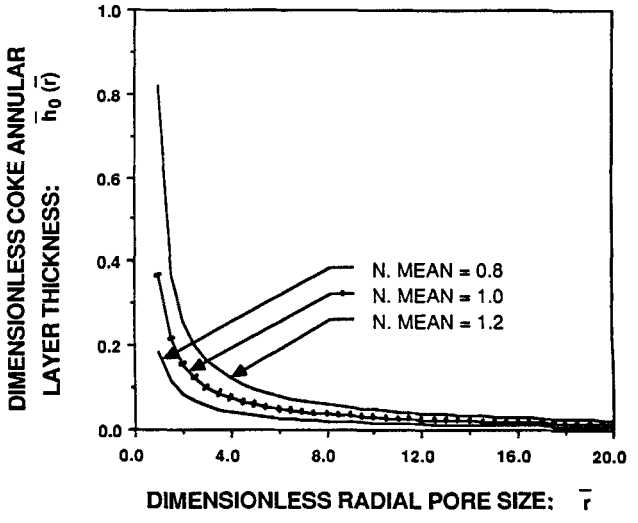

Figure 11. Coke profiles for various pore volume distributions.
Case III, coke volume fraction $\bar{V} = 0.05$
N. Mean, normalized mean

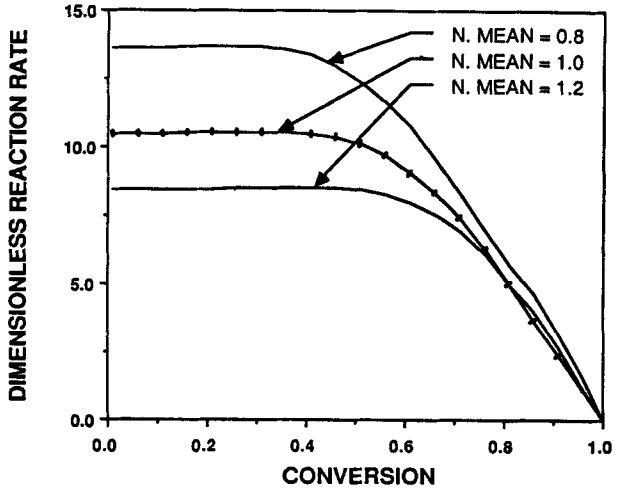

Figure 12. Effect of overall conversion on reaction rates for various pore volume distributions.
Case III, coke volume fraction $\bar{V} = 0.05$
N. Mean, normalized mean.

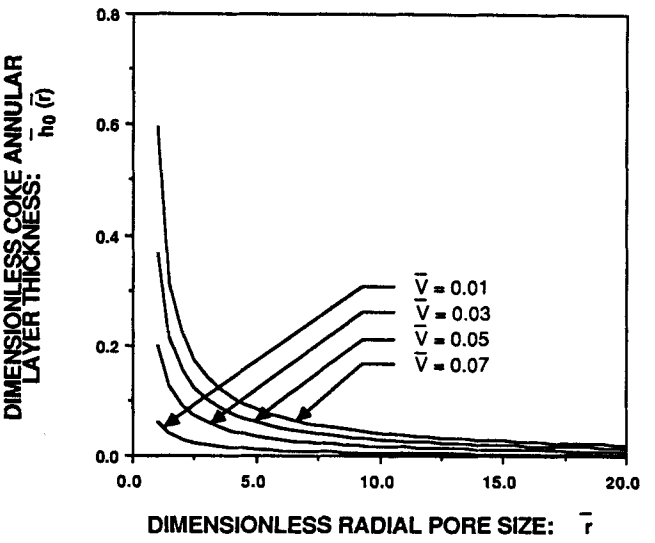

Figure 13. Coke profiles for various levels of coke loading.
Case III; $\bar{V}$, coke volume fraction

volume distribution function. Furthermore, it should be noted that a slight shallow maximum in rate occurs at a lower conversion level for a more dispersed pore structure. This is because the coke layer on a given pore size is thinner in a more dispersed pore structure, as shown in Figure 9, which causes the process of emergence of islands of nonreacting surface of the catalyst to occur at a lower conversion level. The dotted curve in Figures 9 and 10 represents the model results computed for the experiments of Haldeman and Botty.

The computed criterion for no blockage of pore space by coke deposition is listed in Table 2 for each of the pore volume distributions shown in Figure 7. The monotonic increase in the critical $\bar{V}$ with an increase in the variance suggests that the catalyst used in the experiments of Haldeman and Botty would have been more coke-resistant if it had had a pore structure with the same mean in radial pore size but with a more dispersed distribution.

The coke profiles computed for pore volume distributions with different means are presented in Figure 11, based on the distributions shown in Figure 8 and as before for the same coke volume fraction $\bar{V} = 0.05$. Since the overall pore length increases with a decrease in the mean of pore size in pore structure, and for the same reasons as presented above in discussing variance, the coke layer on a given pore size is expected to be thinner in a pore structure comprised of more small pores, as presented in Figure 11. This results in a larger reaction surface area in a pore structure comprised of more small pores and, as illustrated in Figure 12, larger reaction rates as the mean of the distribution function is reduced. As before, a shallow maximum in rate may be found at a lower conversion level. The dotted curve in Figures 11 and 12 represents the model results computed for the experiments of Haldeman and Botty.

Table 3 lists the critical values of $\bar{V}$ for no blockage of pore space by coke deposition for those pore volume distributions shown in Figure 8. The critical $\bar{V}$ increases with a decrease in the mean for the distribution, suggesting that the catalyst used in the experiments of Haldeman and Botty would also have been more coke-resistant if it had had a pore structure with the same degree of radial dispersion but with a smaller mean.

Table 3. Effect of Pore Structure on Criterion for No Blockage of Pore Space

Normalized Mean	Critical $\bar{V}$
0.8	0.1491
1.0	0.0836
1.2	0.0517

Effect of coke loading

The coke profiles computed for different coke levels are presented in Figure 13, showing that for a given pore size the annular coke layer thickness decreasese with a fall in the coke level,

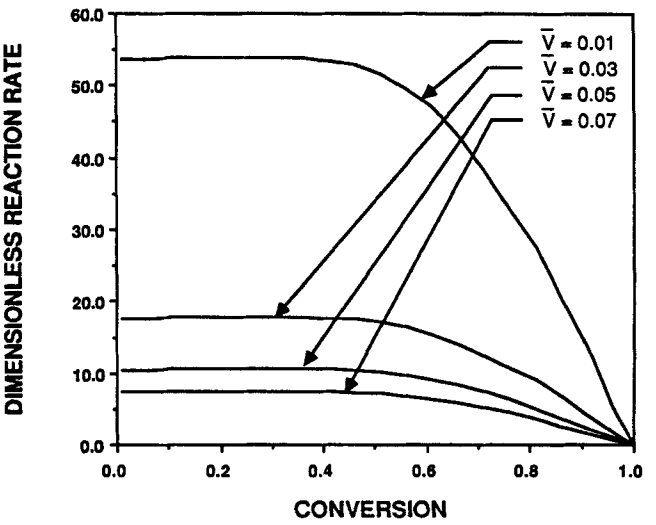

Figure 14. Effect of overall conversion on reaction rates for various levels of coke loading.
Case III; $\bar{V}$, coke volume fraction

and that the change of thickness with coke level is in general more significant in the regime of low coke level ($\bar{V} < 0.03$) than that in the regime of high coke level ($\bar{V} > 0.07$). Consequently, with total pore volume constant and a fixed pore structure, the reaction surface area within a coked catalyst with a lower coke loading is larger than that with a higher coke loading. Furthermore, this effect is more significant in the regime of low coke level. Therefore, as shown in Figure 14, the rate is greater for a lower coke level, and the sensitivity to coke level is more significant at low levels.

Acknowledgment

This research was partly funded by the U.S. Department of Energy under Contract No. DE-AC21-81MC-161.

Notation

a, b = stoichiometric coefficients
A = solid reactant
B = gaseous reactant
C = carbon concentration
C_0 = initial carbon concentration
D = discriminant
$f(r)$ = pore volume distribution of porous media
$G)r)$ = gamma distribution function
$\bar{f}(\bar{r})$ = normalized dimensionless pore volume distribution of porous media
$F(C/C_0)$ = coke burning rate function
F_k = normalization factor
$g(r)$ = pore-distributed volume distribution of solid A
$\bar{g}(\bar{r})$ = normalized dimensionless pore-distributed volume distribution of solid A
$h_0(r)$ = thickness of annular layer of solid A at $t = 0$
$\bar{h}_0(\bar{r})$ = dimensionless thickness of annular layer of solid A at $t = 0$
$h(r, t)$ = thickness of annular layer of solid A at any time
k = integer index, $k = 0, 1, 2$
L = overall pore length of porous media
m = integer index
p, g = stoichiometric coefficients
P = gaseous product
$P(r, t)$ = circumferential surface area of annulus of solid A at any time
$\bar{P}(\bar{r}, \tau)$ = dimensionless circumferential surface area of annulus of solid A at any dimensionless time
P_{ox} = oxygen partial pressure
Q = gaseous product
$Q(r, t)$ = inner surface area of cylinder of solid A at any time
$\bar{Q}(\bar{r}, \tau)$ = dimensionless inner surface area of cylinder of solid at any dimensionless time
r = radial pore size
$\bar{r}$ = dimensionless radial pore size
r_N = smallest radial pore size
r_{E1} = equivalent radius
r_{E2} = equivalent radius
r_W = largest radial pore size
R = ideal gas law constant
R_s = kinetic-controlled surface reaction rate
S = reaction surface area per unit volume in random pore model, or overall pore surface area of porous media
S_0 = S at $t = 0$ random pore model
t = time
$t^*(r)$ = time period for removal of solid A from pores with radii between r and $r + dr$
T = temperature
dv = differential volume of solid A at any time
V = overall pore volume of porous media
$\bar{V}$ = volume ratio of V_R to V
$\bar{V}_c$ = critical $\bar{V}$ for no blockage of pore space
V_R = overall volume of solid A
$V_R^*(t)$ = overall volume of solid A at any time
X = conversion

Greek letters

$\Gamma(\rho)$ = Euler gamma function
Ψ = structural parameter of random pore model
ρ = solid coke density, or parameter of gamma distribution function
λ = parameter of gamma distribution function
μ = mean for gamma distribution function
μ_f = mean for $f(r)$
μ_g = mean for $g(r)$
σ^2 = variance for gamma distribution function
σ_f^2 = variance for $f(r)$
σ_g^2 = variance for $g(r)$
τ = dimensionless time

Literature cited

Androutsopoulos, G. P., and R. Mann, "On the Inevitability of Nonuniform Foulant Deposition within a Catalyst Pellet," *Chem. Eng. Sci.*, **33,** 673 (1978).

Bhatia, S. K., and D. D. Perlmutter, "A Random Pore Model for Fluid-Solid Reactions. I: Isothermal, Kinetic Control," *AIChE J.*, **26,** 379 (1980).

Barrett, E. P., L. G. Joyner, and P. P. Halenda, "The Determination of Pore Volume and Area Distributions in Porous Substances. I: Computations for Nitrogen Isotherms," *J. Amer. Chem. Soc.*, **73,** 373 (1951).

Beeckman, J. W., and G. F. Froment, "Catalyst Deactivation by Active Site Coverage and Pore Blockage," *Ind. Eng. Chem. Fundam.*, **18,** 245 (1979).

———, "Catalyst Deactivation by Site Coverage and Pore Blockage," *Chem. Eng. Sci.*, **35,** 805 (1980).

Chin, G. S., S. Kimura, S. Tone, and T. Otake, "Gasification of Coal Char with Steam. 1: Analysis of Reaction Rate," *Int. Chem. Eng.*, **23,** 105 (1983).

Dutta, S., C. Y. Wen, and R. J. Belt, "Reactivity of Coal and Char. 1: In Carbon Dioxide Atmospheres," *Ind. Eng. Chem. Process Des. Dev.*, **16,** 20 (1977).

Dutta, S., and C. Y. Wen, "Reactivity of Coals and Char. 2: In Oxygen-Nitrogen Atmosphere," *Ind. Eng. Chem. Process Des. Dev.*, **16,** 31 (1977).

El-Kady, F. Y. A., and R. Mann, "Predicted Influence of Pore Structure Modifications for Catalyst Pellets Deactivated by Fouling," *J. Catal.*, **69,** 147 (1981).

Froment, G. F., and K. B. Bischoff, "Nonsteady-State Behavior of Fixed-Bed Catalytic Reactors Due to Catalyst Fouling," *Chem. Eng. Sci.*, **16,** 189 (1961).

———, "Kinetic Data and Product Distributions from Fixed Bed Catalytic Reactors Subject to Catalyst Fouling," *Chem. Eng. Sci.*, **17,** 105 (1962).

Gavalas, G. R., "A Random Capillary Model with Application to Char Gasification of Chemically Controlled Rates," *AIChE J.*, **26,** 577 (1980).

Gates, G. C., J. R. Katzer, and G. C. Schuit, *Chemistry of Catalytic Processes*, McGraw-Hill, New York, 41–45 (1979).

Haldeman, R. G., and M. C. Botty, "On the Nature of the Carbon Deposit of Cracking Catalysts," *J. Phys. Chem.*, **63,** 489 (1959).

Hashimoto, K., K. Miura, F. Yoshikawa, and I. Imai, "Change in Pore Structure of Carbonaceous Materials During Activation and Adsorption Performance of Activated Carbon," *Ind. Eng. Chem. Process Des. Dev.*, **18,** 73 (1979).

Hippo, E., and P. L. Walker, Jr., "Reactivity of Heat-Treated Coals in Carbon Dioxide at 900°C," *Fuel*, **54,** 245 (1975).

Hughes, C. C., and R. Mann, "Interpretation of Catalyst Deactivation by Fouling from Interactions of Pore Structure and Foulant Geometries," *Amer. Chem. Soc. Symp. Ser.*, No. 65, 201 (1978).

Jenkins, R. G., S. P. Nandi, and P. L. Walker, Jr., "Reactivity of Heat-Treated Coals in Air at 500°C," *Fuel*, **52,** 288 (1973).

John, T. M., R. A. Pachovsky, and B. W. Wojciechowski, "Coke and Deactivation in Catalytic Cracking," *Adv. Chem. Ser.*, No. 133, 422 (1974).

Levenspiel, O., "Experimental Search for a Simple Rate Equation to Describe Deactivating Porous Catalyst Particles," *J. Catal.*, **25,** 265 (1972).

Mann, R., F. Y. A. El-Kady, and I. R. Moore, "Deactivation of a Sup-

ported Zeolitic Cracking Catalyst: A Pore Structural Approach," *Ind. Chem. Eng. Symp. Ser.*, No. 87, 25 (1984).
Mann, R., F. Y. A. El-Kady, and R. Marzin, "Catalyst Deactivation by Fouling: A Wedge-Layering Analysis of the Consecutive Reaction," *Chem. Eng. Sci.*, **40**, 249 (1985).
Newson, E., "Catalyst Deactivation Due to Pore Plugging by Reaction Products," *Ind. Eng. Chem. Process Des. Dev.*, **14**, 27 (1975).
Prater, C. D., J. Wei, V. W. Weekman, Jr., and B. Gross, "A Reaction Engineering Case History: Coke Burning in Thermofor Catalytic Cracking Regenerators," *Adv. Chem. Eng.*, **12**, 1 (1983).
Sadana, A., and L. K. Doraiswamy, "Effect of Catalyst Fouling in Fixed-, Moving-, and Fluid-Bed Reactors," *J. Catal.*, **23**, 147 (1971).
Su, J.-L., and D. D. Perlmutter, "Effect of Pore Structure on Char Oxidation Kinetics," *AIChE J.*, **31**, 973 (1985).
Tomita, A., O. P. Mahajan, and P. L. Walker, Jr., "Reactivity of Heat-Treated Coals in Hydrogen," *Fuel*, **56**, 137 (1977).
Voorhies, A., "Carbon Formation in Catalytic Cracking," *Ind. Eng. Chem.*, **37**, 318 (1945).
Weekman V. W., "Kinetics and Dynamics of Catalytic Cracking Selectivity in Fixed-Bed Reactors," *Ind. Eng. Chem. Process Des. Dev.*, **8**, 385 (1969).
Weekman, V. W., and D. M. Nace, "Kinetics of Catalytic Cracking Selectivity in Fixed-, Moving-, and Fluid-Bed Reactors, *AIChE J.*, **16**, 397 (1970).
Weisz, P. B., and R. B. Goodwin, "Combustion of Carbonaceous Deposits within Porous Catalyst Particles," *J. Catal.*, **6**, 227 (1966).
Wojciechowski, B. W., "Kinetic Foundation and Practical Application of TIM on Stream Theory of Catalyst Decay," *Catal. Rev. Sci. Eng.*, **9**, 79 (1974).

Manuscript received July 27, and revision received Dec. 8, 1986.